atmosphere

Article

Influence of the Madden–Julian Oscillation (MJO) on Tropical Cyclones Affecting Tonga in the Southwest Pacific

Moleni Tu'uholoaki [1,2,*], Antonio Espejo [3], Krishneel K. Sharma [4], Awnesh Singh [1], Moritz Wandres [3], Herve Damlamian [3] and Savin Chand [4]

[1] Pacific Centre for Environment and Sustainable Development, The University of the South Pacific, Suva, Fiji; awnesh.singh@usp.ac.fj
[2] Tonga Meteorological Service, Nuku'alofa, Tonga
[3] Geoscience, Energy and Maritime Division, Pacific Community, Suva, Fiji; antonioh@spc.int (A.E.); moritzw@spc.int (M.W.); herveda@spc.int (H.D.)
[4] Centre for New Energy and Transition Research, Federation University, Mt Helen Campus, Victoria, Australia; kk.sharma@federation.edu.au (K.K.S.); s.chand@federation.edu.au (S.C.)
* Correspondence: s11182388@student.usp.ac.fj or molenit@gmail.com

Abstract: The modulating influence of the Madden–Julian oscillation (MJO) on tropical cyclones (TCs) has been examined globally, regionally, and subregionally, but its impact on the island scale remains unclear. This study investigates how TC activity affecting the Tonga region is being modulated by the MJO, using the Southwest Pacific Enhanced Archive of Tropical Cyclones (SPEArTC) and the MJO index. In particular, this study investigates how the MJO modulates the frequency and intensity of TCs affecting the Tonga region relative to the entire study period (1970–2019; hereafter referred to as all years), as well as to different phases of the El Niño southern oscillation (ENSO) phenomenon. Results suggest that the MJO strongly modulates TC activity affecting the Tonga region. The frequency and intensity of TCs is enhanced during the active phases (phases six to eight) in all years, including El Niño and ENSO-neutral years. The MJO also strongly influences the climatological pattern of genesis of TCs affecting the Tonga region, where more (fewer) cyclones form in the active (inactive) phases of the MJO and more genesis points are clustered (scattered) near (away from) the Tonga region. There were three regression curves that best described the movement of TCs in the region matching the dominant steering mechanisms in the Southwest Pacific region. The findings of this study can provide climatological information for the Tonga Meteorological Service (TMS) and disaster managers to better understand the TC risk associated with the impact of the MJO on TCs affecting the Tonga region and support its TC early warning system.

Keywords: tropical cyclones; Madden–Julian oscillations; Tonga; ENSO; Southwest Pacific; island scale

check for updates

Citation: Tu'uholoaki, M.; Espejo, A.; Sharma, K.K.; Singh, A.; Wandres, M.; Damlamian, H.; Chand, S. Influence of the Madden–Julian Oscillation (MJO) on Tropical Cyclones Affecting Tonga in the Southwest Pacific. *Atmosphere* **2023**, *14*, 1189. https://doi.org/10.3390/atmos14071189

Academic Editor: Massimiliano Burlando

Received: 30 May 2023
Revised: 30 June 2023
Accepted: 10 July 2023
Published: 24 July 2023

1. Introduction

The most hazardous and destructive meteorological phenomena that frequently strike tropical areas are tropical cyclones (TCs). Their continual recurrence has hammered the economic and social development of small island countries in the Southwest Pacific (SWP), including Tonga (see [1–3]). Tonga is ranked third in the world in terms of vulnerability to disasters [4], with expected damage valued at US $15.8 million per year (see [5]). Climatologically, Tonga is affected by 2.6 TCs per year (see [6]) and lies in the latitudinal band where TCs normally reach their maximum intensity (see [7]) and extreme TC-induced wave height (see [8]). The number of intense TCs affecting Tonga has also been found to increase, although not statistically significantly (see [6]). Notable TCs that affected Tonga in the past were TC Isaac in 1982, TC Hina in 1997, TC Waka in 2001, TC Heta in 2004, TC Ian in 2014, TC Gita in 2018, and TC Harold in 2020. TC Gita, a category five cyclone, was the most intense TC to ever affect the Tonga region historically, and inflicted damages were equivalent to around 38% of Tonga's gross domestic product (GDP). Category five TC Ian incurred damage equivalent to 11% of Tonga's GDP (see [9]). Recently, TC Harold, another category five cyclone, caused 23% of Tonga's GDP (or US $111 million) worth of damage (see [10]).

The El Niño Southern oscillation (ENSO) and the Madden–Julian oscillation (MJO) are the two dominant modes of climate and intrasesonal variability modulating TC activity in the SWP on interannual and intraseasonal time scales, respectively (see [1,11–15]). Recently, Tu'uholoaki et al. [6] analysed the TC genesis climatology of TCs affecting the Tonga region during ENSO and concluded that El Niño events significantly impact TC genesis, frequency, and location. The influence of the MJO on the frequency and intensity of TCs has also been examined for the wider South Pacific and SWP [13–15] and specific regions of the SWP [11]. However, there has been less emphasis on local-scale TC activity affected by the MJO. Local-scale understanding of TC activity is important to strengthen risk knowledge, inform disaster managers, and improve early warning systems (EWSs) for disaster risk preparedness and mitigation. EWS has been proven to save lives and property and return multiple times more benefits for every dollar invested in it [16].

Briefly, the MJO is a tropical disturbance originating in the Indian Ocean, propagating eastward at 5 m s^{-1} along the equatorial zone and taking between 30- to 60-day intervals to complete a cycle [17,18]. The MJO peaks during austral summer and coincides with the Southern Hemisphere TC seasons. During this time, the South Pacific Convergence zone (SPCZ), the incubator for TC genesis, is also very active (see [12,15]).

The MJO often modulates both the frequency and intensity of TCs globally (see [14,19–21]). For example, Chand and Walsh [11] showed that the frequency and intensity (>category three) of TCs within the Fiji, Samoa, and Tonga (FST) regions are greater during the active phases of the MJO (i.e., phases six, seven, and eight) when the convective activity becomes enhanced over the region. Conversely, TC activity becomes suppressed during the inactive phases of the MJO (phases two and three) over the FST region. Ramsay et al. [13] showed that the combined phases six and seven and eight and one (two and three and four and five) east of 170° E are associated with significantly more (less) TC activity. Klotzbach [14] identified that TC activity is enhanced during the MJO phases six to eight with favourable thermal and dynamical conditions, while Diamond et al. [15] reported 36.7% (17%) during phases six to seven (phases two to three), which accounts for the highest (lowest) proportion of TCs in SWP.

The MJO can also influence the movement of TCs. Chand and Walsh [22] categorised TC genesis in the FST region into three clusters according to the characteristics of the tracks. The first cluster encompassed straight-moving tracks oriented in a northwest-to-southeast direction driven by the mid-level westerly steering winds that are dominant in the SWP, especially east of New Zealand (see [23]). The second group comprised of TC tracks that initially moved eastward before turning southeastward, reflecting TC travelling over the mid-level westerly steering winds before being taken over by the subtropical high-pressure systems to the south (see [1,11]). Lastly, their recurving tracks initially moved southwestward shortly before progressively turning southeastward, indicating TCs travelling around the periphery of the subtropical high to the south. When the steering winds exerted by the subtropical high pressure to the south are weak, the Coriolis force tends to influence the motion of TCs to be more poleward (see [1]).

The MJO not only modulates TCs but also interacts with other weather and climate phenomena such as the SPCZ, Intertropical Convergence Zone (ITCZ), monsoonal troughs, equatorial waves, mid-latitude weather patterns, mesoscale convective systems (see [21,24–26]), and ENSO (see [27–29]). For example, during phases four and five, the convection enhances the atmospheric Rossby waves at mid-latitude, and the Rossby waves, in turn, can enhance the lower-level winds near the surface at 180° E longitude (see [30]); the latter affects TC genesis in the SWP. In addition, the diagonal section of the SPCZ is also enhanced due to upper-level forcing (see [31]). These conditions are favourable for TC genesis and intensification, respectively.

Despite the influence of the MJO on the intensity and frequency of TCs at the regional (3300 km by 10,450 km) and subregional scales (2200 km by 2200 km), the hazardous weather associated with TC impact usually occurs at the local scale (1100 km by 1100 km). Therefore it is worthwhile to explore if the MJO effect on TC at this scale is statistically significant. Since Chand and Walsh [11] examined the large-scale weather patterns in the FST region during MJO and Tu'uholoaki et al. [6] analysed the climatology of the genesis of TCs affecting the Tonga region during ENSO, in the present study, we examine the role of the MJO and how it interacts with the different phases of ENSO to modulate the interannual variability in TC counts and intensities along the Tonga region.

2. Data and Methods

2.1. Track Data and Study Area

We used historical TC tracks from 1969/70 to 2018/19 seasons from the Southwest Pacific Enhanced Archive of Tropical Cyclones dataset (SPEArTC; see [32]). Magee et al. [33] compared three TC databases: the Joint Typhoon Warning Center (JTWC), the International Best Track Archive for Climate Stewardship (IBTrACS), and the Southwest Pacific Enhanced Archive of Tropical Cyclones (SPEArTC). They identified the SPEArTC database as being most suitable for TC analysis in this region. The SPEArTC dataset mainly contains 6-hourly track information comprising positions of the eye (latitudes and longitudes), maximum 10-min averaged winds (knots), and central pressures (hPa). Following Sharma et al. [34], TC genesis is defined as the first track point in the SPEArTC dataset, and TCs are classified according to the combined SWP TC/Australia TC category classification system in Tu'uholoaki et al. [6] (see Table 1). As the TC season in Tonga and the South Pacific regions covers two calendar years (i.e., from November to December of the first calendar year and January to April of the following year), the second year refers to a particular TC season. Since TCs also occurred outside of the TC season, we defined the TC season from 1 July to 30 June the following year.

Table 1. Classification of the SWP TCs combined with the Australian TC category classification system with 10-min averaged wind speed (adopted from Tu'uholoaki et al., [6]).

Classification of Weather Disturbances/Australian TC Category Classification System	Speed Range (Knots)
Tropical depressions	<34
Tropical cyclones (Gale)/Category 1	34–47
Tropical cyclones (Storm)/Category 2	48–63
Severe Tropical cyclones (Hurricane)/Category 3	64–85
Severe Tropical cyclones (Hurricane)/Category 4	86–107

Following Tu'uholoaki et al. [6], we defined the Tonga region as a circle with a radius of 5 degrees centred on Nuku'alofa, the capital of Tonga (Figure 1). The size is chosen given the diameter of TC ranges from 200 to 1000 km (see [35]), and any TCs crossing the circle are considered to have affected Tonga. Figure 1 also shows 128 TCs that affected the Tonga region between 1970 and 2019, with 119 TCs having at least a gale category.

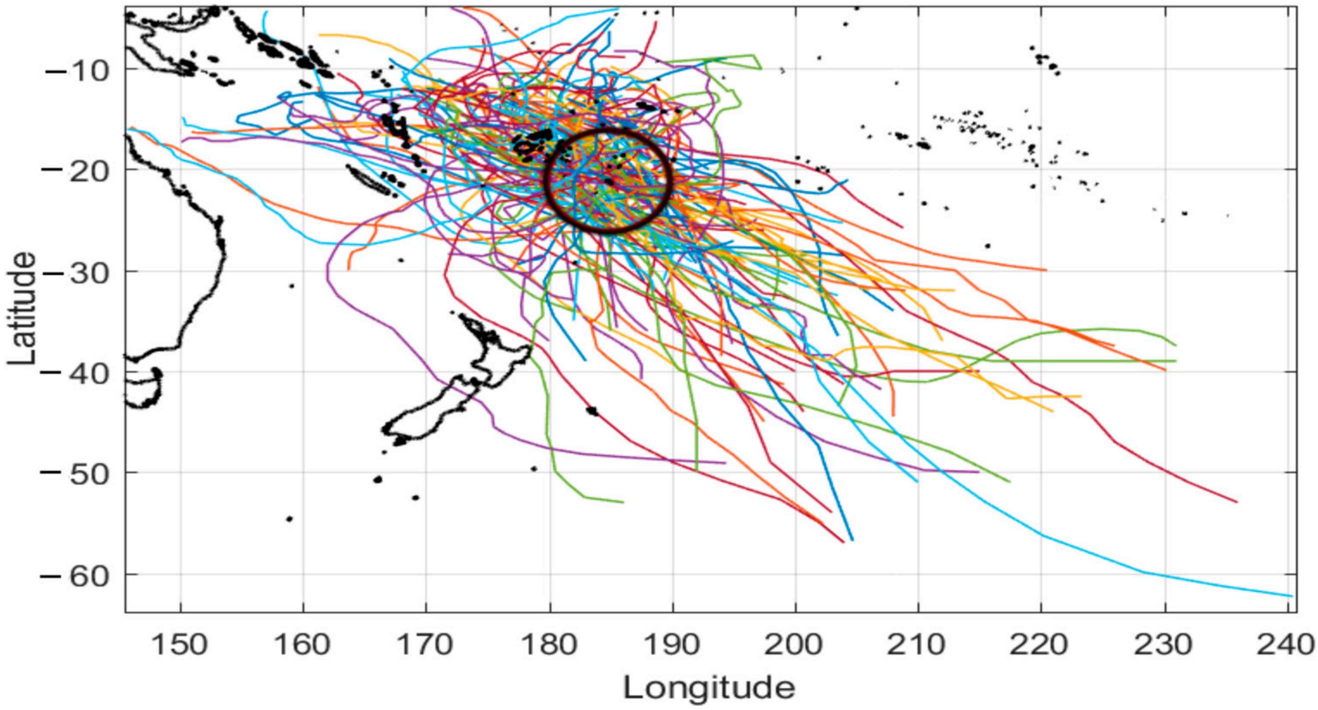

Figure 1. A 5-degree radius circle centred on Nuku'alofa, referred to as the Tonga region, with 128 TC tracks (in coloured plots) passing through the region between 1970–2019.

2.2. Real-Time Multivariate MJO (RMM) Index

The real-time multivariate MJO (RMM) index, developed by Wheeler and Hendon [36] to measure the MJO cycle, is available at the Australian Bureau of Meteorology's website (http://www.bom.gov.au/climate/mjo/; accessed on 20 April 2020) from 1974 to the present day. The RMM index is derived using the first 2 components of the principal component analysis (RMM1 and RMM2) of the combined fields of near-equatorially averaged 850 hPa zonal wind, 200 hPa zonal wind, and satellite-observed outgoing longwave radiation (OLR) data. For continuity of the study, we included the MJO index between 1969 to 1974 from Oliver and Thompson [37], which reconstructed the MJO index developed by Wheeler and Hendon [36] into the early 20th century using 20th century reanalysis (see [38]). The reconstructed MJO index can be obtained online from this address: https://ecjoliver.weebly.com/mjo-reconstruction.html (accessed on 30 May 2020).

South Pacific, FST, and Tonga are favoured for TC activity when the MJO-enhanced activity is located over the Western Pacific (phases 7 and 8) and Western Hemisphere (phase 8) [11,14]. To obtain the large-scale conditions in each MJO phase, following Klotzbach [14], the large-scale environmental field data from November to April of the following year were obtained from the European Centre for Medium-Range Weather Forecasts (ECMWF) ERA5 reanalysis single levels daily on a 1.0° by 1.0° grid. The data were downloaded using the climate data store (CDS) application program interface (API) python script (see the CDS website for more detail; https://cds.climate.copernicus.eu/api-how-to; accessed on 21 June 2023). They are the 200-hPa (U200)(m/s), zonal wind at 850-mb (U850)(m/s), sea surface temperature (SST) (K), sea level pressure (SLP) (hPa), top net thermal radiation (J/m^2)) (equivalent to minus outgoing longwave radiation (OLR)), 300-hPa omega (Pa/s)), 850-hPa relative vorticity (RV850) (10^6/s), and 700-hPa relative humidity (RH700) (%) in the SWP (10° S–20 S, 135° E–210° E). Field values are calculated as deviations from the MJO phase 1–8 average when the MJO index is greater than 1. Values that are significantly different at the 95% level from the phase 1–8 average are highlighted in boldfaced type. The unit in Kelvin was converted to Celsius, J/m^2 to -W/m^2, and Pa/s to hPa/day to be consistent with units used in previous studies (e.g., [14]). The wind shear was derived by removing the U850 winds from U200.

2.3. Oceanic Niño Index (ONI)

We used the Oceanic Niño Index (ONI), which is based on the sea surface temperature (SST) anomalies in the Niño 3.4 region (5° N–5° S, 170° W–120° W), to provide information on the state of the ENSO. The ONI values are obtained by removing the running 3-month average of SST anomalies over the Niño 3.4 region from a 30-year SST anomaly-based period (1986–2015). We classify El Niño (La Niña) years as when the ONI is $\geq$+0.5 °C ($\leq$−0.5 °C) for at least 5 consecutive months. In addition, ENSO-neutral years are defined for the ONI values between these 2 thresholds. We obtained a total of 18, 19, and 13 El Niño, La Niña, and ENSO-neutral years, respectively.

2.4. Bootstrap Method

Since there are only a few TCs (i.e., <30) occurring in each of the MJO phases, the statistical significance of the frequency distribution of each cluster was tested by bootstrapping them against the original sample (following Camargo et al. [39]). The method randomly assigns a TC to each of the MJO phases for 10,000 trials to calculate the statistical significance of the number of TCs for all years, El Niño, La Niña, and ENSO-neutral years. The null hypothesis assumes that the mean of the number of TCs occurred in all 8 phases and the mean of the number of TCs occurred in individual phase are the same.

The bootstrap method is also used to compute the statistical difference at the 95% level between the average of all 8 phases and an individual phase of large-scale environmental fields. The null hypothesis assumes that the difference between the average of all 8 phases and an individual phase of large-scale environmental fields is equal to 0.

2.5. Track Clustering

TC tracks in the Tonga region were examined for relational behaviours in their track types using the objective cyclone track clustering technique as per Gaffney [40]. The method has been successfully used by Camargo et al. [39,41] to study TC tracks in the western North Pacific basin and by Chand and Walsh [11], Sharma et al. [42], and Ramsay et al. [13] for the FST region, the SWP, and the Southern Hemisphere, respectively. The toolbox is available online at this address: http://www.datalab.uci.edu/resources/CCT/ (accessed on 12 February 2021).

The technique builds a mixture of polynomial regression models based on the geographical shape and position of TC track trajectories (curves; see [39–41,43]). The rationale is that each TC track can be assigned to a group or cluster of similar traits using these underlying polynomial regression models.

Chand and Walsh [11] assessed the TC tracks in the FST region in terms of visual inspection and ease of interpretation, and the best trade-off was a second-order polynomial regression model. As per the method used by Gaffen [40], the optimal number of clusters can be determined by assigning each cluster a log likelihood value, which is the probability of the occurrence of each cluster. The corresponding number of clusters with the highest log likelihood probability across a set of clusters is the optimal number. Chand and Walsh [11] found that the optimal number, 3, gives clusters interpretable in the context of the steering mechanisms in the FST region. Following Chand and Walsh [11], once again the best trade-off for the 128 TCs is the second-order polynomial regression model and K = 3 best characterises TC tracks in the Tonga region. This is not unexpected as the Tonga region lies within and occupies about 50% of the FST region.

3. Results and Discussions

3.1. MJO and Climatology of Large-Scale Environmental Fields

Following Klotzbach [14], Table 2 shows values obtained for the large-scale environmental fields (200–850-hPa zonal wind shear, sea surface temperature, sea level pressure, outgoing longwave radiation, 300-hPa omega, 850-hPa relative vorticity, and 700-hPa relative humidity) in the Southwest Pacific (10° S–20° S, 135° E–210° E) for each of the MJO phases when the MJO index was equal to one or more. The bootstrap method is used to compute the statistical difference at the 95% level between the average of all eight phases and an individual phase and is displayed in bold-faced type.

Table 2. Large-scale environmental fields during (a) all years (including El Niño, La Niña, and ENSO-neutral), (b) El Niño, (c) La Niña, and (d) ENSO-neutral years that influence TC genesis and intensity in the Southwest Pacific (10°–20° S, 135° E–210° E) are shown below with corresponding values for each of the MJO phases. These values were obtained by removing the MJO phase one to eight average from the individual MJO phase when the RMM index is greater than one. Values that are significantly different at the 95% level from the MJO phase one to eight average are highlighted in boldfaced type.

	(a) All Years							**(b) El Niño**						
Phase	**$U_{200–850}$**	**SST**	**SLP**	**OLR**	**300 hPa Omega**	**RV_{850}**	**RH_{700}**	**$U_{200–850}$**	**SST**	**SLP**	**OLR**	**300 hPa Omega**	**RV_{850}**	**RH_{700}**
1	**−0.77**	**−0.10**	**1.21**	**0.34**	**6.77**	0.05	**−4.08**	−0.29	**−0.09**	**1.38**	**0.40**	**8.63**	**0.73**	**−4.14**
2	**1.14**	**−0.04**	**1.09**	**0.22**	**8.20**	**1.07**	**−2.00**	**2.5**	**−0.10**	**1.25**	**0.24**	**8.61**	**1.02**	**−2.29**
3	**3.64**	−0.02	**0.38**	**0.19**	**9.63**	**1.63**	**−1.12**	**4.63**	−0.01	**0.78**	**0.23**	**10.96**	**1.58**	**−1.70**
4	**4.03**	0.01	−0.07	**0.06**	**6.14**	**1.34**	**0.91**	**3.97**	−0.04	−0.06	−0.03	2.55	**1.17**	**0.98**
5	**2.09**	**0.06**	**−0.63**	**−0.17**	−2.35	**0.75**	**2.81**	**2.01**	0.05	**−0.49**	**−0.21**	−3.66	**1.33**	**2.58**
6	**−1.41**	**0.06**	**−1.16**	**−0.37**	**−12.61**	**−0.80**	**3.35**	**−2.44**	**0.08**	**−1.22**	**−0.37**	**−12.02**	−0.27	**4.25**
7	**−4.73**	0.03	**−0.98**	**−0.34**	**−14.30**	**−2.40**	**1.76**	**−6.66**	0.06	**−1.48**	**−0.35**	**−14.42**	**−3.50**	**1.72**
8	**−4.00**	−0.01	**0.14**	**0.07**	−1.51	**−1.66**	**−1.63**	**−3.72**	0.05	−0.13	**0.09**	−0.66	**−2.05**	**−1.39**
	(c) La Niña							**(d) ENSO-Neutral**						
Phase	**$U_{200–850}$**	**SST**	**SLP**	**OLR**	**300 hPa omega**	**RV_{850}**	**RH_{700}**	**$U_{200–850}$**	**SST**	**SLP**	**OLR**	**300-hPa omega**	**RV_{850}**	**RH_{700}**
1	**−3.12**	0.01	**0.54**	−0.13	**−9.02**	**−1.36**	−0.05	−0.59	**−0.14**	**1.25**	**0.43**	**9.74**	0.160	**−5.05**
2	−0.47	**0.08**	**0.740**	**0.18**	**6.14**	0.28	**−1.16**	**1.42**	**−0.06**	**1.15**	**0.24**	**8.90**	**1.32**	**−2.24**
3	**2.87**	0.00	−0.100	**0.16**	**9.31**	**1.01**	**−0.99**	**3.55**	−0.03	**0.43**	**0.19**	**9.41**	**1.82**	**−1.01**
4	**3.11**	**0.08**	−0.04	**0.23**	**10.68**	**1.14**	−0.59	**4.47**	0.00	−0.09	**0.04**	**6.39**	**1.53**	**1.26**
5	**4.35**	−0.05	0.0	**0.19**	**10.59**	**1.50**	**−0.42**	**1.54**	**0.09**	**−0.77**	**−0.23**	**−4.52**	**0.45**	**3.59**
6	0.97	**−0.08**	**−0.91**	**−0.280**	**−11.29**	**−0.73**	**2.23**	**−1.81**	**0.11**	**−1.17**	**−0.40**	**−13.07**	**−1.00**	**3.45**
7	**−3.83**	0.04	**−0.60**	**−0.31**	**−11.69**	**−0.76**	1.45	**−4.25**	0.03	**−0.94**	**−0.34**	**−15.02**	**−2.67**	**1.86**
8	**−3.88**	−0.07	**0.37**	−0.04	**−4.72**	**−1.10**	−0.47	**−4.32**	−0.01	0.15	**0.06**	−1.82	**−1.61**	**−1.85**

Climatologically, Table 2 a shows wind shear, sea surface temperature, upper-level divergence, mid-level humidity, and low-level vorticity during active phases six to eight deviated significantly at the 95% level from the phase one to eight average and are favourable conditions for TC activity, except for the upper-level divergence in phase eight and SST in phases seven and eight. In contrast, wind shear (phases two to five), sea surface temperature (phases one to two, five), OLR (phases one to four), upper-level divergence (phases one to four), relative vorticity (phases two to five), and relative humidity (phases one to three) during the MJO inactive phase deviated significantly at the 95% level and are unfavourable conditions for TC activity. These results reinforce previous findings that large-scale environmental conditions are favourable for TC genesis in the SWP during active phases and suppressed during other phases (see [11,14]). In addition, generally, similar large-scale conditions for the MJO active phase during El Niño, La Niña, and ENSO-neutral years favouring TC activity in contrast to the MJO inactive phase with conditions unfavourable for TC activity (see Table 2 b–d, respectively).

A case study of the large-scale conditions that coincided with the genesis of six TCs that affected Tonga during El Niño, La Niña, and ENSO-neutral years is shown in Table 3. Three of those were severe TCs (TCs Ron, Gita, and Kina). The large-scale conditions observed when they reached severe TC intensity are also shown. Regardless of the strengths of TCs, MJO, and ENSO phases, favourable conditions for TC genesis, such as low-level vorticity (negative), SST (positive), negative OLR, and upper divergence (negative), were observed. However, relative humidity was slightly less during TC Urmil (category two) that occurred during an ENSO-neutral year with the MJO phase equal to three. A decreasing wind shear and an increasing upper-level divergence relative to previous days are ideal conditions for TC intensification. TCs Ron, Gita, and Kina intensified into a category five, five, and four, respectively. Relative to the conditions on the day of genesis, wind shear dropping was 4.76, 0.9, and 7.1 m/s and upper-level divergence rising was 27.16, 14.64, and 0.45 hPa/day, respectively, which explains the favourable conditions for their intensification.

Table 3. Similar to Table 2 but for large-scale environmental conditions for six TCs affecting Tonga, two TCs are selected from each ENSO phase, with one being a severe TC. The red box represents EL Niño, blue for La Niña, and green for ENSO-neutral.

TCs	Category	Date	Mjophase	$U_{200-850}$	SST	SLP	OLR	300-hPa Omega	RV_{850}	RH_{700}	ENSO Phase
Lola	1	4 Apr 2016	4	−10.88	0.63	−4.10	−0.68	−6.48	−3.01	10.42	
Ron	1	1 Jan 1998	6	−4.97	0.09	−1.64	−0.72	−27.09	−6.99	8.71	
Ron	5	7 Jan 1998	8	−9.73	−0.07	−3.08	−1.69	−74.25	−9.00	6.96	
Elisa	2	7 Jan 2008	6	−9.31	0.18	−1.54	−1.49	−43.17	−6.20	17.65	
Gita	1	1 Feb 2018	7	−6.63	0.54	−3.34	−0.94	−25.52	−9.28	13.87	
Gita	5	12 Feb 2018	7	−7.53	0.32	−2.68	−0.07	−40.16	−1.94	−6.74	
Urmil	2	13 Jan 2006	3	−1.67	0.37	−2.42	−0.56	−16.67	−2.53	−2.22	
Kina	1	26 Dec 1992	7	1.69	−0.31	−3.58	−0.69	−35.39	−4.87	0.47	
Kina	4	1 Jan 1993	7	−8.80	−0.39	−4.29	−1.08	−35.84	−12.9	−1.96	

3.2. MJO and TC Frequency

TC genesis has been observed to occur in all phases of the MJO between 1970–2019 (Figure 2a) with about 8.8%, 8.0%, 5.6%, 10.8%, 7.5%, 18.2%, 19.5%, and 21.6% for MJO phases one to eight, respectively. TC genesis in phases six to eight is about 60% higher than those occurring in other phases. In particular, the peak number of TCs in phases seven and eight are statistically significant at 95% and 99%, respectively (Figure 2a, all years). This is not surprising, as shown in Table 2 and in previous studies, large-scale environmental conditions are favourable for TC genesis in the SWP, whereas they are suppressed and unfavourable during other phases. Figure 2a also shows that the MJO active phases six to eight continue to be favourable over the Tonga region during El Niño (72.1%; significant at 99% for phase eight) and ENSO-neutral years (56.8%; significant at 95% for phase seven) but with a lesser impact during La Niña (49.2%). The least number of TCs during La Niña in contrast to other phases is mainly due to fewer TCs formed during phase six relative to other phases (see phase six in Figure 2b). This can be explained by enhanced vertical wind shear and lower sea surface temperatures (statistically significant at 96% level) in phase six compared to other phases (see Table 2 c), hence suppressed TC genesis during La Niña years. In addition, it can be seen during La Niña years that only a few TC geneses formed near 170° E compared to El Niño and ENSO-neutral years (see Figure 5c in Tu'uholoaki et al. [6]) as the mean TC genesis shifts south and southwestward. On the contrary, a higher TC genesis near 170° E is observed during El Niño years, coinciding with the southeastward steering winds in phase six, which may explain the higher frequency of TCs affecting the Tonga region during phase six of El Niño years. This may be due to the sea surface temperature, relative humidity, outgoing long wave radiation, and upper-level divergence being enhanced in phase six during El Niño (see Table 2 b; statistically significance at 95% level). Consistent with Chand and Walsh [11], the genesis maxima for phase six in the FST region lies around 170° E and is closely associated with El Niño.

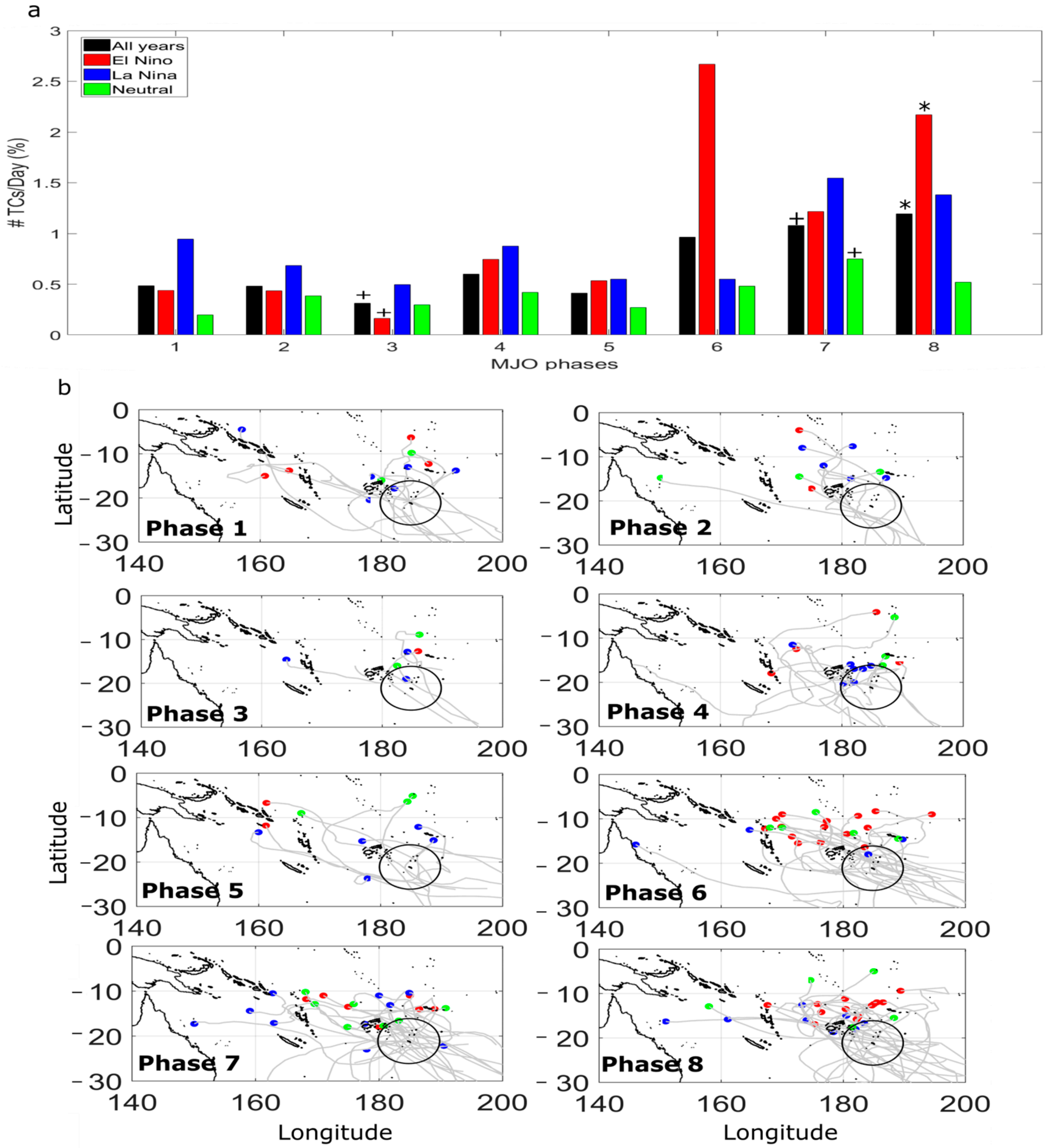

Figure 2. (**a**) Number of TC geneses per day (%) during 1970 and 2019 for all years (in black), El Niño years (in red), La Niña years (in blue), and ENSO-neutral years (in green). (**b**) The spatial distribution of genesis points (El Niño years (in red), La Niña years (in blue), and ENSO-neutral years (in green)) and corresponding tracks for the eight MJO phases. Asterisk (*) and plus (+) signs in (**a**) indicate statistical significance at 99% and 95% levels, respectively.

In addition, the relatively larger west-to-east extension of the TC genesis spatial distribution for the ENSO-warm phase and ENSO-neutral phase (see [6]) may mirror the propagation of the MJO from phase six in the west to phase eight in the east of the tropical Pacific. In contrast, during La Niña, the spatial distribution of TC genesis is confined to a relatively smaller area east of 173° E (see [6]), reflecting the dominance of phases seven and eight over phase six (Figure 2). This explains why La Niña exerts the least impact on TC genesis compared with its counterparts during active phases of the MJO.

Consistent with previous findings (see [11]), TC genesis probability in the Tonga region increases during the active phases (six to eight) compared to inactive phases (one to five) regardless of ENSO state.

3.3. MJO and Spatial Distribution of TC Genesis

The spatial distribution of genesis points is scattered and further apart when there is fewer TC genesis during inactive phases (one to five) in contrast to being more clustered together and closer to Tonga during the active phases (six to eight) of the MJO (Figure 2b). TC genesis points during El Niño (La Niña) are more equatorward (northwest-westward) relative to the Tonga region due to the northeastward (southwestward) movement of the SPCZ (see [6,12,15]). Additionally, it can be seen that most of the TCs affecting Tonga formed outside and away to the far northwest of the region (Figure 2b), highlighting the importance of the steering winds, which primarily influence TC movements (see [1]).

To obtain the dominant relational behaviour of TC movements affecting Tonga, we assessed 128 TC tracks, and results indicate that the second-order polynomial regression provides the best fit for the FST region, consistent with Chand and Walsh, [22]. Since the number of clusters can be determined subjectively, various values of K = 1–5 were inspected, and K = 3 provided the optimal results. Particularly, the three mean regression curves obtained from K = 3 remained stable even with different iterations. However, when the K values were increased to four, five, and six, the clusters appeared to split into smaller but more refined clusters.

Following Chand and Walsh [11], TC tracks were grouped into three clusters using the second-order regression model (Figure 3). Cluster one (Figure 3b) prevails with 58.6% of the considered tracks, comprising TCs formed to the northwest and then tracked towards the Tonga region by the mid-tropospheric westerly winds (see [1,7,11,23]). Figure 3c shows cluster two (29.7% TC tracks) with TCs that were generally steered south towards Tonga before abandoning the region as they curve around the periphery of the subtropical high to the south. Cluster three (Figure 3d) has the least number of TCs with 11.7%, generally tracking east-to-southeastward from the Coral Sea driven by the mid-level westerly winds towards the Tonga region and then around the periphery of the subtropical high belt to the south when leaving the area (see [1,11]).

In clusters one, two, and three, about 24.2%, 10.9%, and 3.1% occurred during El Niño compared to 20.3%, 10.2%, and 7.8% during La Niña and 14.1%, 8.6%, and 0.8% during ENSO-neutral years, respectively. More genesis points formed equatorward and closer to the Tonga region can explain why clusters one and two slightly dominate during El Niño years, whereas cluster three dominates La Niña years as TC genesis mean position shifts more poleward and westward (see [6]). These findings reinforce previous studies in this area. For example, a cluster with a straight-oriented northwest-to-southeast regression track, similar to cluster one, was also obtained by Ramsay et al. [13] to represent all TC tracks east of 170° E in the South Pacific. They found that this cluster is significantly more frequent during El Niño compared to La Niña years. They also found that TC genesis in this area is suppressed when the MJO is located over the Indian Ocean and maritime continent (i.e., inactive phases). Sharma et al. [42] grouped SWP TC tracks into five clusters, with their clusters two and four being similar to clusters one and two in the present study, respectively. They are all associated with El Niño and geographically originate from a similar region. In addition, in the study by Sharma et al. [40], cluster one is similar to cluster three, with both clusters associated with La Niña, geographically originating in the same region, the Coral Sea, and possessing longer trajectories.

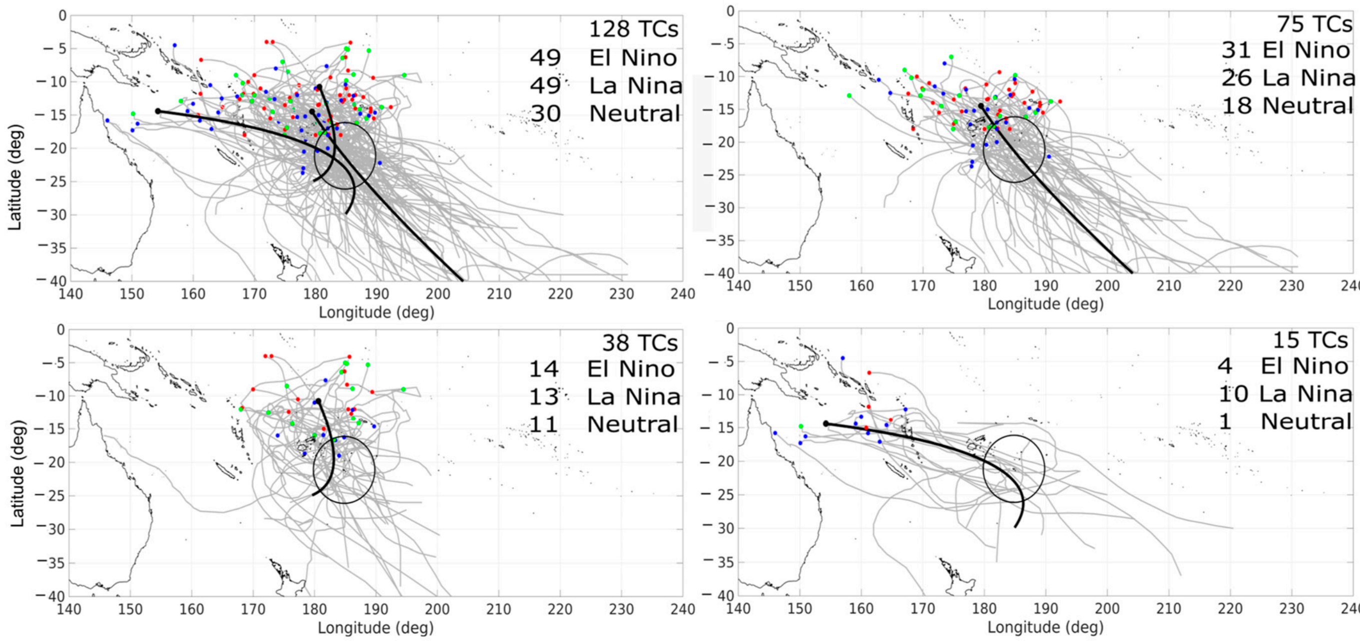

Figure 3. The spatial distribution of TC genesis points (El Niño in red, La Niña in blue, and ENSO-neutral in green) and the accompanied tracks corresponding with each of the clusters of TCs affecting Tonga. Mean regression curves (thick black lines) are also shown.

Figure 3 illustrates the high sinuosity (deviation from straight lines) of the TC tracks that characterise TCs in the South Pacific. Sharma et al. [42] classified tracks affecting Tonga's exclusive economic zone (EEZ) to be mostly straight and quasi-straight, and this can be seen in clusters one and three. Cluster two is more recurving and sinuous. Sinuous and recurving TC tracks are more threatening owing to their complex and convoluted shapes and therefore increase the risk of multiple landfalls. This sinuosity contributes to greater longevity and intensity (see [44]), which at most times poses forecasting challenges due to their erratic movement and most often makes them reach full strength by the time they reach Tonga (see [6]), which lies in the latitude band (~20° S) where TCs in the SWP reach their maximum intensity (see [7]).

3.4. MJO and TC Intensity

The climatology of TC classification in each phase of the MJO (Figure 4) shows that hurricane and gale categories are enhanced during active phases of the MJO (phases six to eight), attributed to active convection as shown in Table 2 and reported by Chand and Walsh [11] for the FST region. The number of TCs with gale, storm, or hurricane intensity peaks significantly at phases six, seven, and eight, at 95%, 95%, and 99%, respectively. In particular, the co-influence of El Niño during active MJO tends to enhance TCs up to hurricane intensity during phases six and eight, while hurricanes during phase seven are enhanced during La Niña—all significant at 95% (Figure 4b,c). This can be attributed to vertical wind shear values favourable for intensification (i.e., wind shear less than 4 m/s; see [45]) at phases six and eight (−2.44 and −3.72 m/s, respectively; see Table 2 b) during El Niño and favourable upper-level divergence and vertical wind shear at phase seven during La Niña (see Table 2 c). During ENSO-neutral years (Figure 4d), hurricane-level TCs are common during phase eight of the MJO (significant at 99%). This can be attributed to favourable wind shear being statistically significant at the 95% level in phase eight compared to others (see Table 2 d). In addition, this result is consistent with earlier findings that the Tonga region lies in the latitude band where TCs reach their maximum intensity (see [6,7]). Furthermore, TCs with storm intensity are enhanced during active phases of the MJO, peaking at phase seven (statistically significant at the 95% level during El Niño years). Moreover, more gale intensity TCs occur during MJO active phases and ENSO-warm-neutral years (phase six, significant at the 95% level during ENSO-neutral years). Interestingly, during La Niña years, more gale intensity TCs formed during inactive phases than active phases, with the majority of these TCs forming within the vicinity of the Tonga region (see phase four in Figure 2b). This may be due to the upper-level forcing that enhanced low-level winds in the region near 180° E longitude during phases four and five of the MJO (see [30]), which in turn favours low-level vorticity, one of the favourable conditions for TC genesis (see [46]). Additionally, the presence of high vertical wind shear during the inactive phase (see phases one to five in Table 2) may prevent these TCs from reaching their maximum intensity, highlighting that more TCs does not necessarily mean stronger TCs.

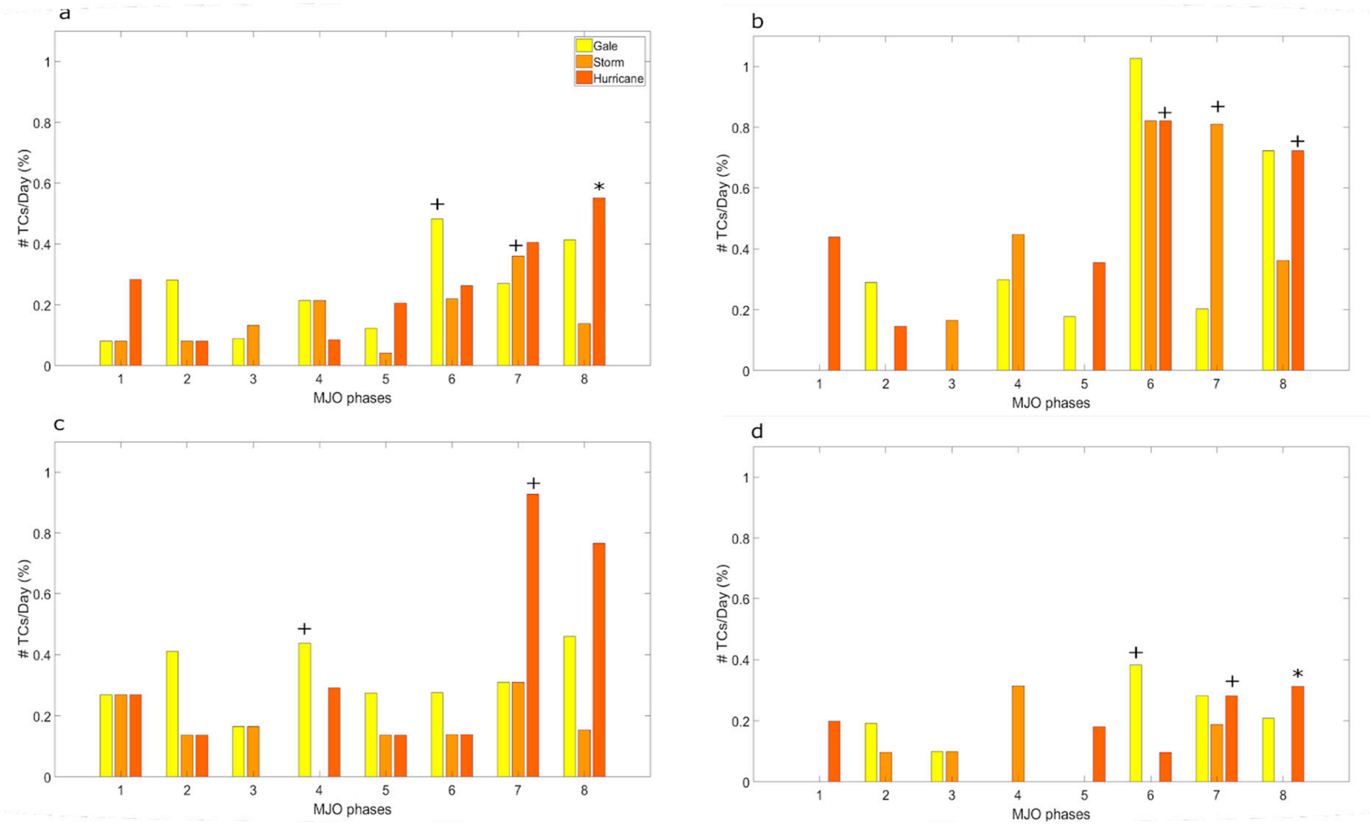

Figure 4. Frequency by TC intensity during the different phases of the MJO for (**a**) all years, (**b**) El Niño years, (**c**) La Niña years, and (**d**) ENSO-neutral years within the Tonga region between 1970–2019. Asterisk (*) and plus (+) signs indicate statistical significance at the 99% and 95% level, respectively.

3.5. MJO and TC Trends

Tonga is affected by 2.6 TCs per year for all years as well as in La Niña years, increasing to 2.8 during El Niño years [6]). In addition, the trend for the number of TCs is decreasing at a rate of 0.0225/0.0002/0.0095/0.0128 TCs per year during all years/El Niño/La Niña/ENSO-neutral years, though not statistically significant (null hypothesis being that there is no trend).

The trend for the number of TCs occurring during the MJO active phase (phases six to eight; see Figure 5) is −0.0286/0.0027/−0.0108/−0.0085 TCs/year for all years/El Niño/La Niña/ENSO-neutral years. All are not significant at the 95% level except for the trend during El Niño, which is not only statistically significant but also increasing. This finding supports the claim by Chand et al. [47] that El Niño-driven TC activity in the central South Pacific, including Fiji and Tonga regions, is projected to increase in the future.

Hence, this MJO active phase may plausibly play a role in and be considered as a subject for further studies.

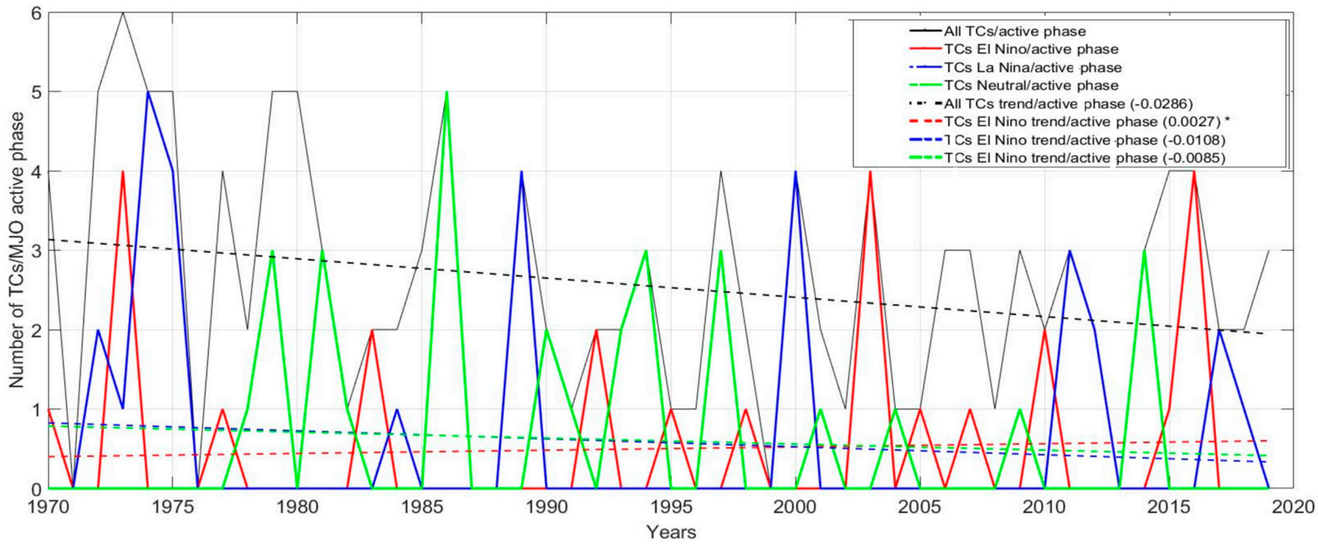

Figure 5. Trends of frequency of TCs per MJO active phase (phases six to eight) for (a) all years (black dashed line), (b) El Niño years (red dashed line), (c) La Niña years (blue dashed line), and (d) ENSO-neutral years (green dashed line) within the Tonga region between 1970–2019. Asterisk (*) sign indicates statistical significance at the 95% level, respectively.

4. Conclusions

This study investigates how TC activity is modulated by the MJO and ENSO combined phases within the Tonga region, emphasising TC frequency and intensity using the SPEArTC database, RMM index, and the ONI. A probabilistic clustering technique was utilised to isolate TC tracks into distinct groups to evaluate the primary cyclone tracks affecting the Tonga region. In addition, the study also examines the climatology (all years and ENSO years) of the large-scale field data favourable for TC genesis and intensification in the SWP.

Although forecasters at the Tonga Meteorological Service (TMS) may be well aware of the relationship between the MJO and TCs that is being monitored by the Australian Bureau of Meteorology and NOAA on a weekly basis and from previous research on the MJO-TC relationship on the regional and subregional scale (Fiji, Samoa and Tonga), no quantitative research has been undertaken to quantify the effect of the MJO on Tonga-region TCs at a local scale. The MJO recurrence and predictability within 30–50 days is vital information for preparation at least three weeks earlier during the TC season. Information about the climatology and variability of the TC–MJO relationship will help the early warning system of TMS.

Results suggest that the MJO strongly modulates TC activity affecting the Tonga region, with more TCs during active phases and less during inactive phases. Similarly, during warm and neutral phases of ENSO, more TCs occur, coinciding with the active phases. On the contrary, lower TCs evolve during La Niña due to the southward displacement of TC genesis, missing the mean mid-level westerly winds steering TCs toward Tonga. The frequency and intensity of gale and hurricane category TCs were enhanced during the active phases (phases six to eight) of the MJO due to favourable large-scale conditions. The MJO also strongly influences the climatological pattern of genesis of TCs affecting the Tonga region, where more (fewer) cyclones form in the active (inactive) phases of the MJO. The findings of this study can provide climatological information for the TMS and decision makers to better understand how the TC risk is modulated by the MJO. These findings greatly contribute to the development of more accurate and actionable TC seasonal outlooks in Tonga. Finally, this methodology could be applied to other local areas where the MJO plays an important role in modulating TC activities.

Author Contributions: Conceptualisation, M.T.; methodology, M.T., A.E., A.S., S.C. and K.K.S.; software, M.T., S.C., K.K.S. and A.E.; validation, M.T., S.C., K.K.S. and A.E.; formal analysis, M.T. and A.E.; investigation, M.T.; resources, A.S. and H.D.; data curation, M.T., A.S. and A.E.; writing—original draft preparation, M.T.; writing—review and editing, M.T., K.K.S., S.C., A.S., A.E. and M.W.; visualisation, M.T. and A.E.; supervision, A.S., H.D., A.E., M.W. and S.C.; project administration, A.S.; funding acquisition, H.D. All authors have read and agreed to the published version of the manuscript.

Funding: The first author was supported by the Pacific Scholarship for Excellence in Research and Innovation (PSERI) from The University of the South Pacific, Fiji.

Institutional Review Board Statement: This study did not require ethical approval.

Informed Consent Statement: Not applicable.

Data Availability Statement: Data used in this study are all publicly available. MJO index are available at http://www.bom.gov.au/climate/mjo/ and https://ecjoliver.weebly.com/mjo-reconstruction.html. Tropical cyclone tracks from SPEArTC dataset is available at http://apdrc.soest.hawaii.edu/projects/speartc/. Large Scale Atmospheric data from European Centre for Medium-Range Weather Forecasts (ECMWF) ERA5 reanalysis single levels daily on a 1.0° by 1.0° grid can be downloaded using the climate data store (CDS) application program interface (API) python script (see the CDS website for more detail; https//cds.climate.copernicus.eu/api-how-to).

Acknowledgments: We thank the COSPPac project for funding the publication of this research. We thank Ashneel Chandra, a student in Climate Dynamics at the Geophysical Institute, University of Bergen, for assisting in downloading the data from ECMWF.

Conflicts of Interest: The authors declare no conflict of interest.

References

1. Terry, J.P. *Tropical Cyclones: Climatology and Impacts in the South Pacific*; Springer Science & Business Media: New York, NY, USA, 2007.
2. Lavender, S.L.; Dowdy, A.J. Tropical cyclone track direction climatology and its intraseasonal variability in the Australian region. *J. Geophys. Res. Atmos.* **2016**, *121*, 13–236. [CrossRef]
3. Magee, A.D.; Verdon-Kidd, D.C.; Kiem, A.S.; Royle, S.A. Tropical cyclone perceptions, impacts and adaptation in the Southwest Pacific: An urban perspective from Fiji Vanuatu and Tonga. *Nat. Hazards Earth Syst. Sci.* **2016**, *16*, 1091–1105. [CrossRef]
4. Radtke, K.; Weller, D. The WorldRiskIndex 2021. Available online: https://reliefweb.nt/report/world/worldriskreport-2021-focus-social-protection (accessed on 18 May 2023).
5. World Bank. Acting on Climate Change and Disaster Risk for the Pacific, World Bank Report, 16. 2013. Available online: https://www.worldbank.org/content/dam/Worldbank/document/EAP/Pacific%20Islands/climate-change-pacific.pdf (accessed on 18 May 2023).
6. Tu'uholoaki, M.; Singh, A.; Espejo, A.; Chand, S.; Damlamian, H. Tropical cyclone climatology, variability, and trends in the Tonga region, Southwest Pacific. *Weather. Clim. Extrem.* **2022**, *37*, 100483. [CrossRef]
7. Dowdy, A.J.; Qi, L.; Jones, D.; Ramsay, H.; Fawcett, R.; Kuleshov, Y. Tropical cyclone climatology of the South Pacific Ocean and its relationship to El Niño–Southern Oscillation. *J. Clim.* **2012**, *25*, 6108–6122. [CrossRef]
8. Stephens, S.A.; Ramsay, D.L. Extreme cyclone wave climate in the Southwest Pacific Ocean: Influence of the El Niño Southern Oscillation and projected climate change. *Glob. Planet. Chang.* **2014**, *123*, 13–26. [CrossRef]
9. World Trade Organisation. Executive Summary. WTO. Report. 2018. Available online: https://www.wto.org/english/tratop_e/devel_e/study_1_pacific_country_annex_18_april_draft_final.pdf (accessed on 18 May 2023).
10. Cyclone Harold. 2020. Available online: https://en.wikipedia.org/wiki/Cyclone_Harold (accessed on 26 May 2023).
11. Chand, S.S.; Walsh, K.J. The influence of the Madden–Julian oscillation on tropical cyclone activity in the Fiji region. *J. Clim.* **2010**, *23*, 868–886. [CrossRef]
12. Vincent, E.M.; Lengaigne, M.; Menkes, C.E.; Jourdain, N.C.; Marchesiello, P.; Madec, G. Interannual variability of the South Pacific Convergence Zone and implications for tropical cyclone genesis. *Clim. Dynam.* **2011**, *36*, 1881–1896. [CrossRef]
13. Ramsay, H.A.; Camargo, S.J.; Kim, D. Cluster analysis of tropical cyclone tracks in the Southern Hemisphere. *Clim. Dyn.* **2012**, *39*, 897–917. [CrossRef]
14. Klotzbach, P.J. The Madden–Julian oscillation's impacts on worldwide tropical cyclone activity. *J. Clim.* **2014**, *27*, 2317–2330. [CrossRef]

15. Diamond, H.J.; Renwick, J.A. The climatological relationship between tropical cyclones in the southwest pacific and the Madden–Julian Oscillation. *Int. J. Climatol.* **2015**, *35*, 676–686. [CrossRef]
16. Fakhruddin, B.S.; Schick, L. Benefits of economic assessment of cyclone early warning systems-A case study on Cyclone Evan in Samoa. *Prog. Disaster Sci.* **2019**, *2*, 100034. [CrossRef]
17. Zhang, C. Madden-julian oscillation. *Rev. Geophys.* **2005**, *43*, 1–46. [CrossRef]
18. Zhang, C. Madden–Julian oscillation: Bridging weather and climate. *Bull. Am. Meteorol. Soc.* **2013**, *94*, 1849–1870. [CrossRef]
19. Schreck, C.J.; Molinari, J.; Aiyyer, A. A global view of equatorial waves and tropical cyclogenesis. *Mon. Weather Rev.* **2012**, *140*, 774–788. [CrossRef]
20. Balaguru, K.; Leung, L.R.; Hagos, S.M.; Krishnakumar, S. An oceanic pathway for Madden–Julian Oscillation influence on Maritime Continent Tropical Cyclones. *Npj Clim. Atmos. Sci.* **2021**, *4*, 52. [CrossRef]
21. Diamond, H.J.; Schreck, C.J., III; Allgood, A.; Becker, E.J.; Blake, E.S.; Bringas, F.G.; Camargo, S.J.; Chen, L.; Coelho, C.A.S.; Fauchereau, N.; et al. The Tropics. *Bull. Am. Meteor. Soc.* **2022**, *103*, S193–S256. [CrossRef]
22. Chand, S.S.; Walsh, K.J. Tropical cyclone activity in the Fiji region: Spatial patterns and relationship to large-scale circulation. *J. Clim.* **2009**, *22*, 3877–3893. [CrossRef]
23. Sinclair, M.R. Extratropical transition of southwest Pacific tropical cyclones. Part I: Climatology and mean structure changes. *Mon. Weather Rev.* **2002**, *130*, 590–609. [CrossRef]
24. Tu'uholoaki, M. Analysis of 8 February Heavy Rainfall Event Over Tongatapu: A Thesis Submitted to the Victoria University of Wellington in Partialfulfilment of the Requirements for the Degree of Master of Science in Geophysics. Master's Thesis, Victoria University of Wellington, Wellington, New Zealand, 2012.
25. Lee, J.C.K.; Lee, R.W.; Woolnough, S.J.; Boxall, L.J. The links between the Madden-Julian Oscillation and European weather regimes. *Theor. Appl. Climatol.* **2020**, *141*, 567–586. [CrossRef]
26. Lin, H. The Madden-Julian Oscillation. *Atmos. Ocean.* **2022**, *60*, 338–359. [CrossRef]
27. Roulston, M.S.; Neelin, J.D. The response of an ENSO model to climate noise, weather noise and intraseasonal forcing. *Geophys. Res. Lett.* **2000**, *27*, 3723–3726. [CrossRef]
28. Zavala-Garay, J.; Zhang, C.; Moore, A.M.; Kleeman, R. The linear response of ENSO to the Madden–Julian oscillation. *J. Clim.* **2005**, *18*, 2441–2459. [CrossRef]
29. Arcodia, M.C.; Kirtman, B.P.; Siqueira, L.S. How MJO teleconnections and ENSO interference impacts US precipitation. *J. Clim.* **2020**, *33*, 4621–4640. [CrossRef]
30. Rui, H.; Wang, B. Development characteristics and dynamic structure of tropical intraseasonal convection anomalies. *J. Atmos. Sci.* **1990**, *47*, 357–379. [CrossRef]
31. Kiladis, G.N.; Wheeler, M. Horizontal and vertical structure of observed tropospheric equatorial Rossby waves. *J. Geophys. Res. Atmos.* **1995**, *100*, 22981–22997. [CrossRef]
32. Diamond, H.J.; Lorrey, A.M.; Knapp, K.R.; Levinson, D.H. Development of an enhanced tropical cyclone tracks database for the southwest Pacific from 1840 to 2010. *Int. J. Climatol.* **2012**, *32*, 2240–2250. [CrossRef]
33. Magee, A.D.; Verdon-Kidd, D.C.; Kiem, A.S. An intercomparison of tropical cyclone best-track products for the southwest Pacific. *Nat. Hazards Earth Syst. Sci.* **2016**, *16*, 1431–1447. [CrossRef]
34. Sharma, K.K.; Verdon-Kidd, D.C.; Magee, A.D. Decadal variability of tropical cyclogenesis decay in the southwest. *Pac. Int. J. Climatol.* **2020**, *40*, 2811–2829. [CrossRef]
35. WMO. Tropical Cyclones. 2022. Available online: https://public.wmo.int/en/our-mandate/focus-areas/natural-hazards-and-disaster-risk-reduction/tropicalcyclones#:~:text=Its%20diameter%20is%20%20typically%20around,storm%20resources%20and%20coastal%20flooding (accessed on 20 December 2022).
36. Wheeler, M.C.; Hendon, H.H. An all-season real-time multivariate MJO index: Development of an index for monitoring and prediction. *Mon. Weather Rev.* **2004**, *132*, 1917–1932. [CrossRef]
37. Oliver, E.C.; Thompson, K.R. A reconstruction of Madden–Julian oscillation variability from 1905 to 2008. *J. Clim.* **2001**, *25*, 1996–2019. [CrossRef]
38. Compo, G.P.; Whitaker, J.S.; Sardeshmukh, P.D.; Matsui, N.; Allan, R.J.; Yin, X.; Gleason, B.E.; Vose, R.S.; Rutledge, G.; Bessemoulin, P.; et al. The twentieth century reanalysis project. *Q. J. R. Meteorol. Soc.* **2001**, *137*, 1–28. [CrossRef]
39. Camargo, S.J.; Robertson, A.W.; Gaffney, S.J.; Smyth, P.; Ghil, M. Cluster analysis of typhoon tracks. Part I: General properties. *J. Clim.* **2007**, *20*, 3635–3653. [CrossRef]
40. Gaffney, S.J. *Probabilistic Curve-Aligned Clustering and Prediction with Regression Mixture Models*; University of California: Irvine, CA, USA, 2004.
41. Camargo, S.J.; Robertson, A.W.; Gaffney, S.J.; Smyth, P.; Ghil, M. Cluster analysis of typhoon tracks Part II: Large-scale circulation, E.N.S.O. *J. Clim.* **2007**, *20*, 3654–3676. [CrossRef]
42. Sharma, K.K.; Magee, A.D.; Verdon-Kidd, D.C. Variability of southwest Pacific tropical cyclone track geometry over the last 70 years. *Int. J. Climatol.* **2021**, *41*, 529–546. [CrossRef]
43. Gaffney, S.J.; Robertson, A.W.; Smyth, P.; Camargo, S.J.; Ghil, M. Probabilistic clustering of extratropical cyclones using regression mixture models. *Clim. Dyn.* **2007**, *29*, 423–440. [CrossRef]
44. Terry, J.P.; Gienko, G. Developing a new sinuosity index for cyclone tracks in the tropical South Pacific. *Nat. Hazards* **2011**, *59*, 1161–1174. [CrossRef]

45. Gray, W.M. Global view of the origin of tropical disturbances and storms. *Mon. Weather Rev.* **1968**, *96*, 669–700. [CrossRef]
46. Paterson, L.A.; Hanstrum, B.N.; Davidson, N.E.; Weber, H.C. Influence of environmental vertical wind shear on the intensity of hurricane-strength tropical cyclones in the Australian region. *Mon. Weather Rev.* **2005**, *133*, 3644–3660. [CrossRef]
47. Chand, S.S.; Tory, K.J.; Ye, H.; Walsh, K.J. Projected increase in El Niño-driven tropical cyclone frequency in the Pacific. *Nat. Clim. Chang.* **2017**, *7*, 123–127. [CrossRef]